Scanning Microscopy

Volume 4 | Number 2 Article 7

6-11-1990

The Development of Dendritic Carbides in a Dual-Phase martensitic/Ferritic Steel

E. Materna-Morris
Institut für Material-und Festkörperforschung

Follow this and additional works at: https://digitalcommons.usu.edu/microscopy

 Part of the Life Sciences Commons

Recommended Citation

Materna-Morris, E. (1990) "The Development of Dendritic Carbides in a Dual-Phase martensitic/Ferritic Steel," *Scanning Microscopy*: Vol. 4 : No. 2 , Article 7.
Available at: https://digitalcommons.usu.edu/microscopy/vol4/iss2/7

This Article is brought to you for free and open access by the Western Dairy Center at DigitalCommons@USU. It has been accepted for inclusion in Scanning Microscopy by an authorized administrator of DigitalCommons@USU. For more information, please contact digitalcommons@usu.edu.

Scanning Microscopy, Vol. 4, No. 2, 1990 (Pages 287-296)
Scanning Microscopy International, Chicago (AMF O'Hare), IL 60666 USA

0891-7035/90$3.00+.00

THE DEVELOPMENT OF DENDRITIC CARBIDES IN A DUAL-PHASE MARTENSITIC/FERRITIC STEEL

E.Materna-Morris

Kernforschungszentrum Karlsruhe, Institut für Material- und Festkörperforschung
Postfach 3640, D-7500 Karlsruhe 1, Federal Republic of Germany
Phone No. 49-7247-822162

(Received for publication March 8, 1990, and in revised form June 11, 1990)

Abstract

Several ferritic-martensitic laboratory melts with a varying chromium content of 9 - 14 wt.% and delta-ferritic quantities ranging from 0 - 25% were investigated by means of impact-testing. The negative influence of delta-ferrite (>0.5%) on the mechanical properties can be explained by the formation of dendritic $M_{23}C_6$-precipitates around the delta-ferrite grains. The development of these dendrites was studied as a function of the cooling kinetics using dilatometric and metallographic measurements and by SEM (scanning electron microscopy) and TEM (transmission electron microscopy) investigations.

Key words: Dual-phase steel, stainless steel, martensite, ferrite, microstructure, precipitates, dendrites, scanning electron microscopy, transmission electron microscopy, continuous cooling transformation diagram, impact bending test.

Introduction

Martensitic-ferritic steels were chosen in addition to austenitic stainless steels as an alternative core structural material for nuclear power plants. As far as the aspect of safety, is concerned, a high impact toughness and low ductile-to-brittle transition temperature (DBTT) are important prerequisites for this application. Furthermore, the material should be easily workable and machinable, e.g., by hardening or welding. For this purpose, about 2 or 3% delta-ferrite seems to be reasonable. Higher delta-ferrite contents, however, have negative effects on yield stress and tensile strength. Up to now, the influence of delta-ferrite has only been described in a contradictory manner (1, 2, 6, 7, 8, 9, 10).

Within the framework of an investigation program of laboratory melts, martensitic steel with different contents of delta-ferrite were studied. All materials were subjected to impact testing with a view to obtain a sufficient data on fracture behaviour during dynamic loads. The emphasis was put on the analysis of the influence of delta-ferrite and its grain boundary carbides. Both, structure and fracture surfaces of impact tested samples were investigated systematically with regard to the mechanical properties.

Experiment

On the basis of the heat resistant Nb-containing steel DIN 1.4914, a dual-phase system of martensite and ferrite was manufactured by varying the chromium content from 9 up to 14 wt.%. The detailed chemical compositions of the laboratory melts are shown in Table 1. Delta-ferrite contents of 0, 0.5, 5, 20 and 25% were achieved. The dependency of delta-ferrite quantities of the alloying elements on the basic structure of Cr-Ni-stainless steels is shown by the Schaeffler diagram given in Fig.1.

Table 1. The chemical composition of the alloys [wt.%].

Charg. Nr.	C1	C2	C3	C4	C5	C6
C	0.13	0.13	0.13	0.135	0.14	0.14
Si	0.38	0.34	0.34	0.34	0.33	0.30
Mn	0.66	0.65	0.62	0.61	0.60	0.62
P	0.006	0.006	0.005	0.006	0.006	0.006
S	0.004	0.004	0.004	0.005	0.004	0.004
Cr	9.15	10.03	11.03	12.10	13.00	14.00
Ni	0.67	0.65	0.63	0.65	0.64	0.64
Mo	0.61	0.60	0.59	0.59	0.59	0.58
V	0.28	0.28	0.26	0.28	0.26	0.27
Nb	0.18	0.17	0.17	0.19	0.18	0.18
Al	0.075	0.100	0.070	0.097	0.090	0.085
B	0.005	0.005	0.004	0.0046	0.004	0.004
N	0.006	0.004	0.005	0.004	0.004	0.005
Co	0.005	0.005	0.004	0.004	0.002	0.002
Cu	0.01	0.01	0.014	0.015	0.01	0.014
Ti	0.005	0.006	0.005	0.006	0.006	0.006
δ-ferrite content [%]	0	0	0.5	5	20	25

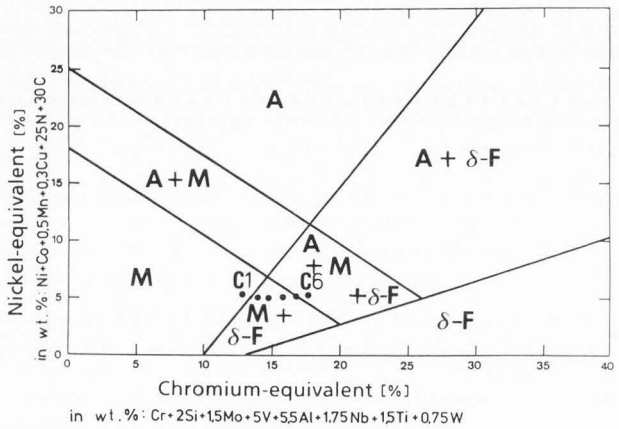

Fig.1. Schaeffler diagram. Effect of alloying elements on the basic structure of Cr-Ni stainless steels; A = austenite, M = martensite, δ-F = delta-ferrite, C1....C6= melts C1, C2, C3, C4, C5, C6.

The double vacuum melted material was supplied as 25 mm square bars. From these bars Charpy-V-notched (CVN) samples (Iso-V-samples in accordance with DIN 50117) were machined with the notch being perpendicular to forging direction. The CVN samples were austenitized at 1075°C for a period of 30 min, cooled in air, tempered at 700°C for 2 h and again subjected to air cooling.

The CVN-impact energies of all melts are given as a function of test temperature. The samples were tested at temperatures ranging from -80° to +160°C to determine the DBTTs (Ductile To Brittle Transition Temperature).

The CVN-samples were examined by instrumented impact-bending tests (13). As a result, a load-time curve is obtained, which is then converted into a load-bending curve. The area integral under the load-bending curve corresponds to the energy spent on the sample during the test. Samples with the same impact energy can differ considerably while subjected to load-bending.

Additionally, a second series of test melts was prepared to investigate the cooling kinetics or structural development at different cooling velocities after austenitization. Dilatometric measurements of the melts were carried out. On the basis of the changes in volume, the tranformation of structure, inclusions and carbides can be determined. After heating to 1075°C, the material was quenched, e.g., in NaOH, or cooled very slowly by means of furnace-cooling. The change in the structure was studied by dilatometric measurements and can be shown in the CCT (continuous cooling transformation) diagram.

The fracture modes of the broken samples were determined using the scanning electron microscope (SEM; SEM 505, Philips) equipped with an energy dispersive x-ray analyzing system (EDX; EDAX). The structures of the materials were investigated by light microscopical (LM), SEM and transmission electron microscopical (TEM) methods. The hardness was measured by Vickers.

Metallographic cuts were prepared from the melts after they had been subjected to standard heat treatments as well as from the samples with the different cooling velocities. To show the different phases and carbides, the cuts were polished and etched using an alcoholic picric acid (400 ml ethyl alcohol, 10 g picric acid, 6 ml hydrochloric acid). With this solution depth etching was carried out to make visible the structure of the delta-ferrite and the carbides.

In addition, chemical extractions were performed with the same chemical solution. After the complete dissolution of the matrix and partial dissolution of the delta-ferrite, the carbides were collected by filtering. This extract was analysed by x-ray diffraction methods.

The microstructure of ultra-thin samples was studied using TEM (EM 400T, Philips), equipped with EDX (EDAX) and STEM-technique (Scanning-TEM). A 10 vol% perchloric acid in 70 vol.% ethyl alcohol and 20 vol.% ethylene glycol solution was used as the elctrolyte (11). The investigations were carried out at room-temperature and 27 Volts using TENUPOL polishing device. The 3 mm-TEM-samples of this material are strongly ferromagnetic. It was therefore necessary to minimize their mass to reduce the influence on the astigmatism in the TEM. Using 1 mm diameter punch, the thin area around the hole

was punched out. The 1 mm diameter samples were then fixed between a sandwich-Cu-grid.

Experimental Results

As can be seen in Fig.2, the charpy impact energy curves can be divided into the regions of the lower shelf, the transition temperature (DBTT) and the upper shelf. The fracture of samples of the lower shelf is transgranular and mostly brittle. At transition temperature the fractures appear in a mixed mode, as is evident in Fig.3B. The rims of the fracture areas are ductile (Fig.4A) and only the central part which covers about 50% of the fracture surface, is brittle. But in higher SEM-magnifications ductile dimples are indicated by the abrupt drops between the cleavage areas in the centre of the fracture surface, Fig.5A. This mode is termed transgranular mixed fracture. The fractures of the upper shelf are mostly ductile. The surface is covered with transgranular dimple formations.

The DBTT values can be determined from the charpy impact curves as 50% of the upper shelf value minus the lower shelf value, Fig.2. With increasing chromium content, the DBTT temperatures increase. The upper shelf energie decreases from 230 to 150 Joule. There is only one exception to the general observation: the melt with a 11 wt.% chromium content (0.5% delta-ferrite), which shows the best behaviour with respect to the DBTT, Fig.6.

In Fig.3A, the load versus bending curve is shown together with the corresponding fracture, Fig.3B. The drop in the curve corresponds to the unstable fracture energy in the centre of the fracture surface.

With the increasing delta-ferrite content a greater tendency to cleavage fracture was observed and DBTT was increased.In the middle length cuts, cleavage fracture was observed preferentially in the delta-ferrite grains, Fig.5B. In the ductile parts of the fractures, the dimples are formed around the boundary carbides. The delta-ferrite as well as the martensite formed ductile tips on the fracture surface, Fig.4B.

The melts with a chromium content of 9 and 10 wt.% show a fully developed martensitic lath structure. In the materials with the higher chromium contents, the delta-ferrite is visible as large grains which are aligned along the forging direction. The grain boundaries are lined with precipitates. The prior austenitic grain sizes in all melts have a diameter of 30±10 μm (ASTM grain size = 7.5±1).

The hardness shown in Fig.7 decreases with higher delta-ferrite contents, but the delta-ferrite itself is distinctly softer than the martensite.

By TEM the typical martensite lath structure can be seen. The delta-ferrite, with its massive carbides on the grain boundaries is clearly visible, Fig.8. The chromium content of the delta-ferrite is 1-2.5 wt.% higher than that of martensite, as was determined by EDX (STEM).

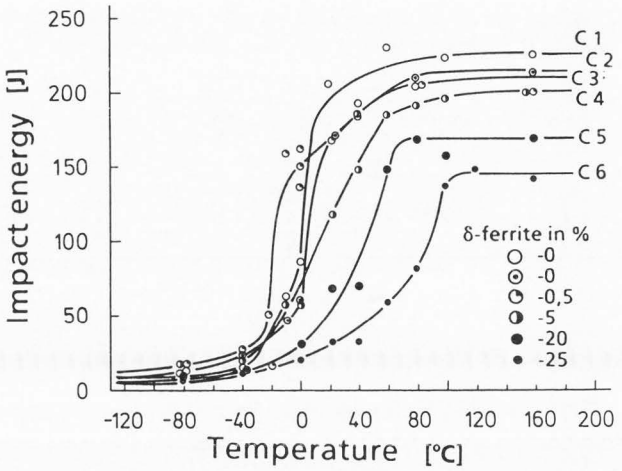

Fig.2. The Charpy V-notch impact energy curves for the different melts.

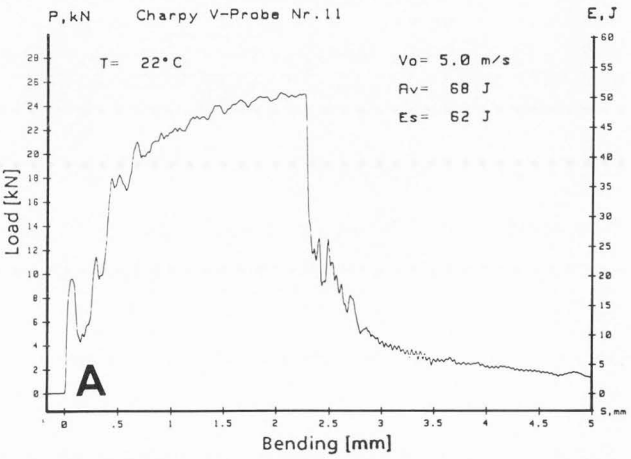

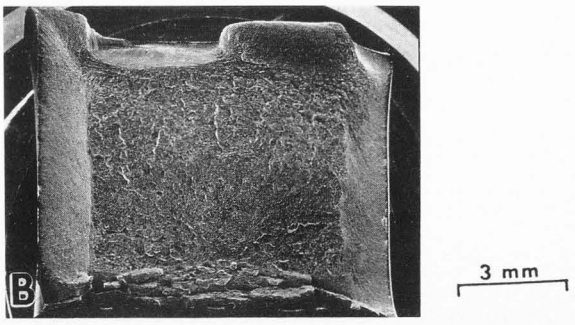

Fig.3. A load versus bending curve of an instrumented impact test during RT and the corresponding fracture surface for the melt C5.

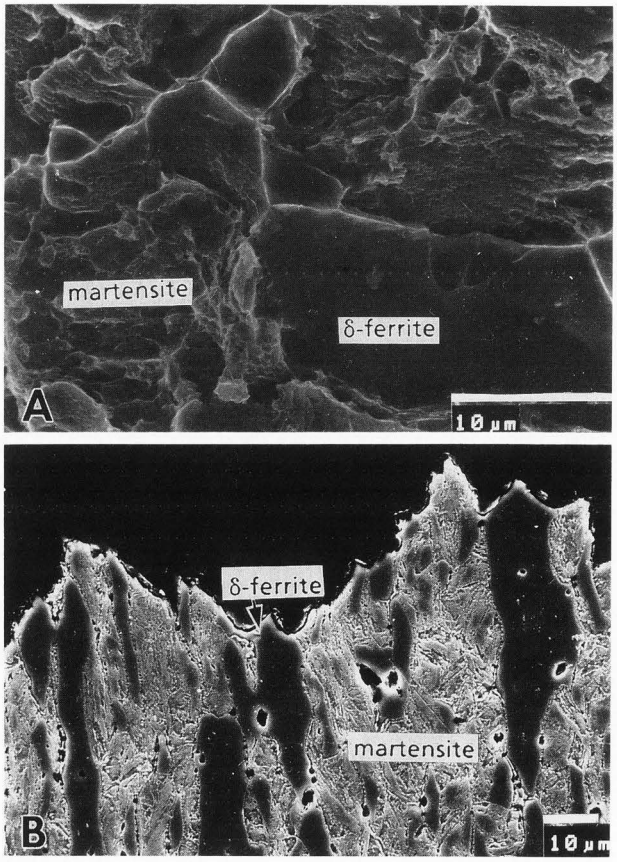

Fig.4.

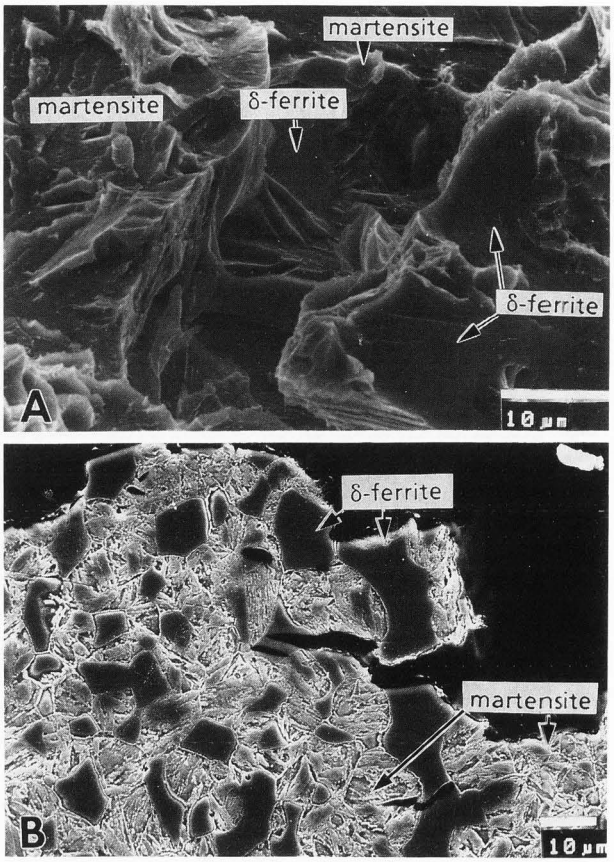

Fig.5.

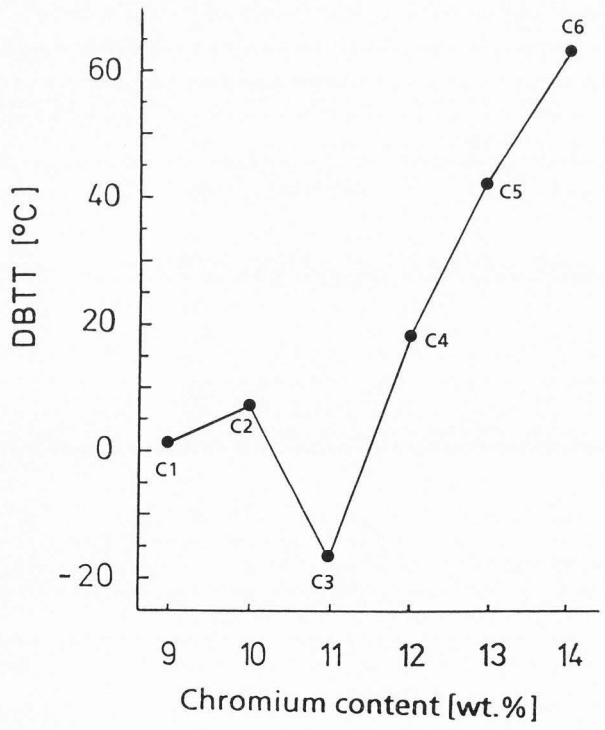

Fig.6.

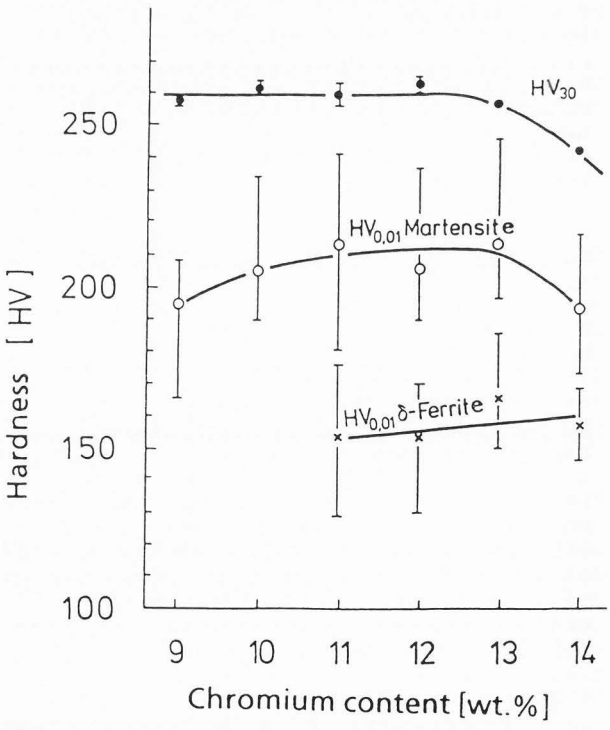

Fig.7.

Fig.4. The ductile deformed delta-ferrite (melt C6) nearby the notch, tested at RT, A) the fracture surface and B) the middle-length cut.

Fig.5. The cleavage fracture of the delta-ferrite (melt C6) in the centre of the fracture, A) the fracture surface and B) the middle-length cut.

Fig.6. A comparison of the DBTT values of the different melts.

Fig.7. The hardness of the alloys and their phases.

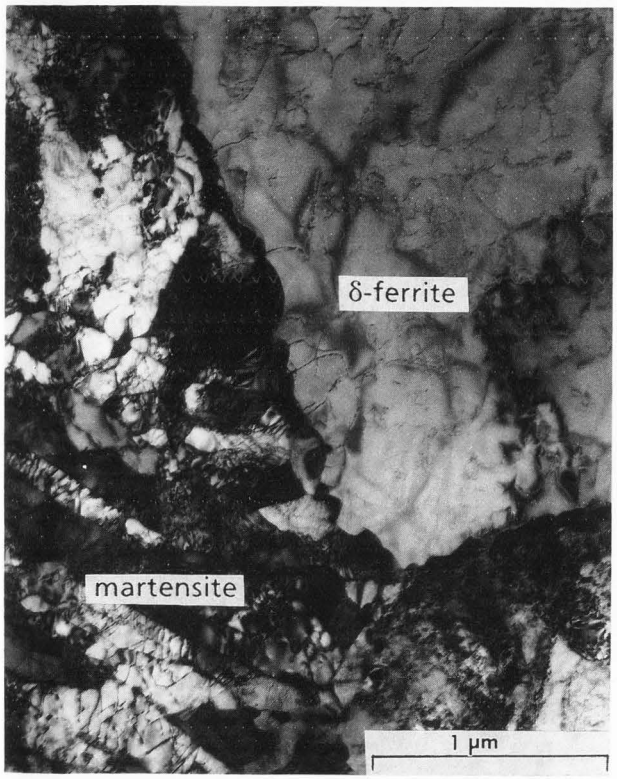

Fig.8. TEM-micrograph, an overview of the carbidic phase boundary delta-ferrite/martensite (melt C5).

The precipitates are mainly of the $M_{23}C_6$ type with two variations: one type has a higher chromium content in the metal part (60-70 wt.% Cr, 25-30 wt.% Fe, 2-3 wt.% V and 3 - 5 wt.% Mo) whereas that of the other is reduced (23-26 wt.% Cr, 68-75 wt.% Fe, 1 wt.% V and 2-2.5 wt.% Mo). The first variation is mostly found on the delta-ferrite edges. In contrast to this, the chromium-depleted phase is observed more in the lath grain boundaries of the martensite. Another type of precipitate, the MX (NbC), is homogeneously distributed in the material, but can also be found in rows within the delta-ferrite.

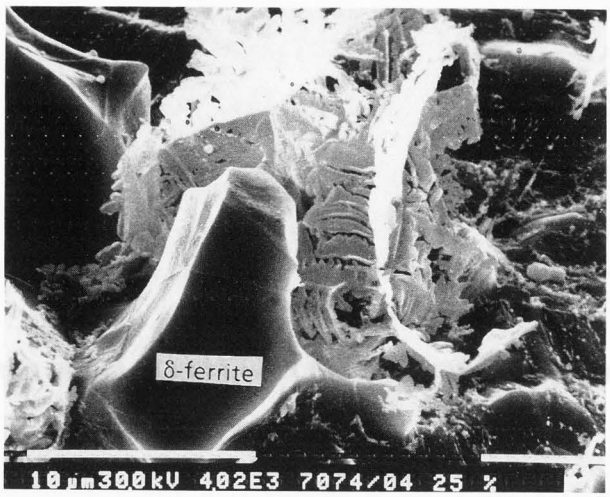

Fig.9. A SEM-micrograph of a dendritic envelopment of a delta-ferrite grain (melt C6).

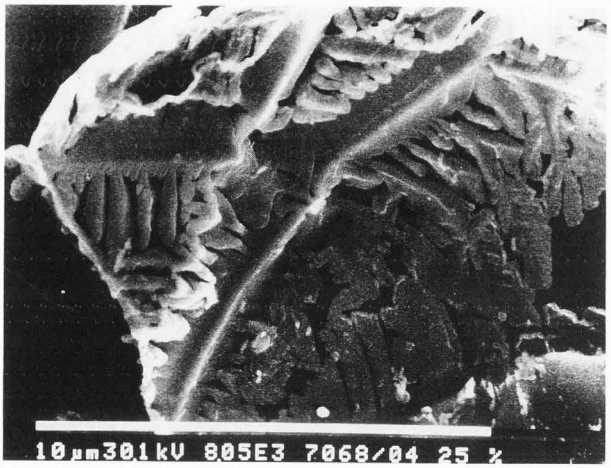

Fig.10. A dendritic formation of $M_{23}C_6$.

The analysis of these precipitates was confirmed by the x-ray diffraction analysis of the chemical extractions.

Deeply etched specimens played a special role with regard to the precipitation behaviour. The carbides lie free and the surrounding material is dissolved. In the materials with more than 5% delta-ferrite, the grain boundary carbides of the delta-ferrite appear as dendritic structures. They increase with the increasing volume of the delta-ferrite portion. In the melt with 25% delta-ferrite the ferrite grains are enveloped completely by the dendritic carbides, Figs.9 and 10. The dendrite walls have a thickness of 0.5-1.0 µm with an average diameter of the ferrite grains of 10 - 20 µm.

These dendritic carbides contribute

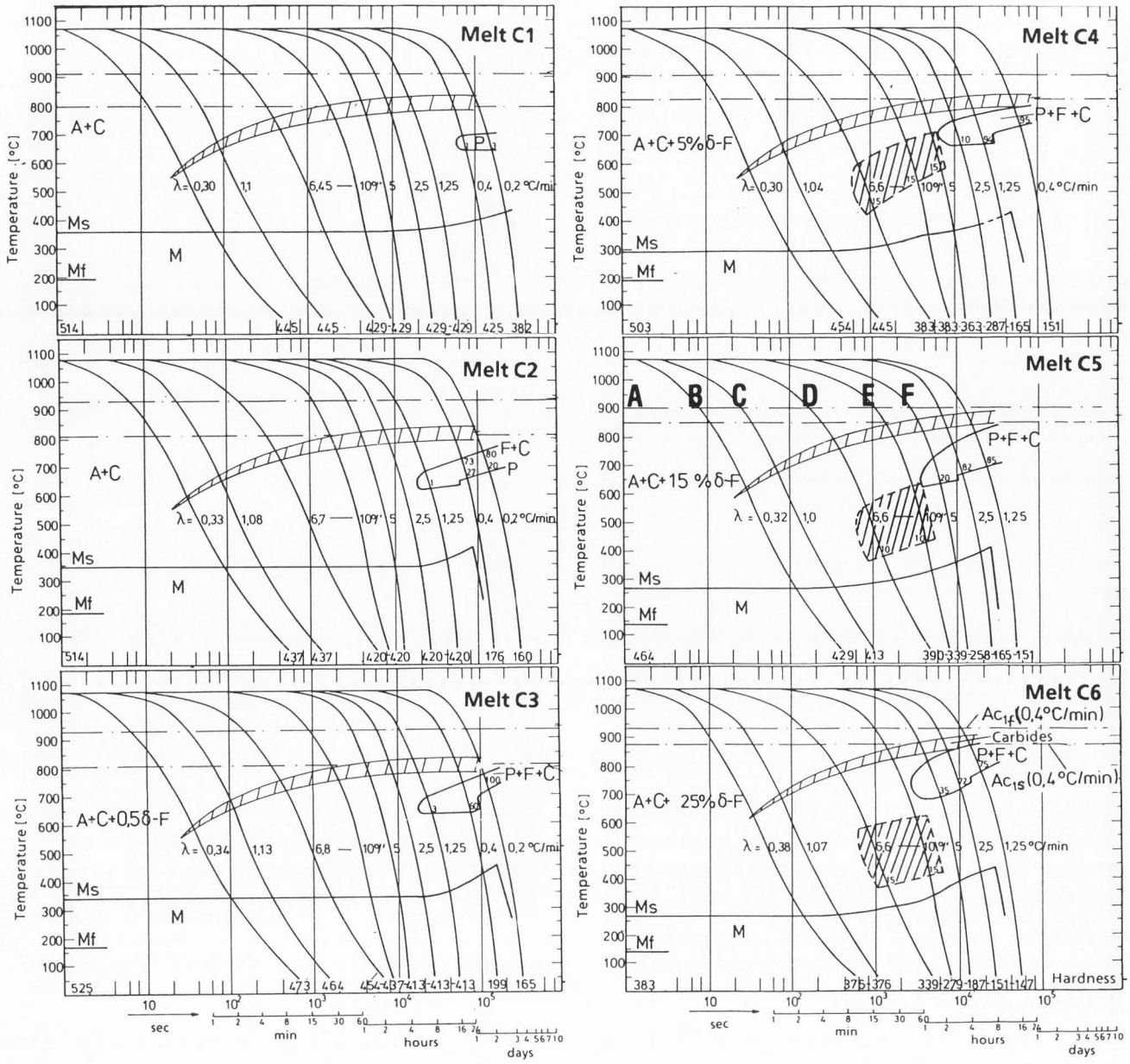

Fig.11. The CCT diagrams of the alloys; A=austenite, C=carbide, δ-F=delta-ferrite, F=ferrite, P=perlite, M=martensite.

to a large extent to the fracture occurrence as is recognized by fracture analysis (12).

Detailed information about the kinetics and the transformation of the structures can be drawn from the CCT diagrams, Fig.11. For each melt eight samples were cooled down from 1075°C. The different cooling rates were recorded. They show the transformation from austenite (A) to martensite (M, M_S=martensite start, M_f=martensite finish). The value of M_S decreases with higher chromium content. The hardness is shown for each curve. It was not only influenced by the chromium content or the delta-ferrite, but also by the cooling rate.

The phases of delta-ferrite (δ -F), carbide (C), perlite (P), and ferrite (F), and the hardness of metallographic cuts were determined. No delta-ferrite was found in melts C1 and C2. Some traces, about 0.5%, were detected in melt C3. The massive formation of delta-ferrite is indicated by the dilatometer curve for a cooling parameter of λ =6.6 (λ = Cooling period from 800° to 500°C in 10^{-2}sec). The change of the structure can

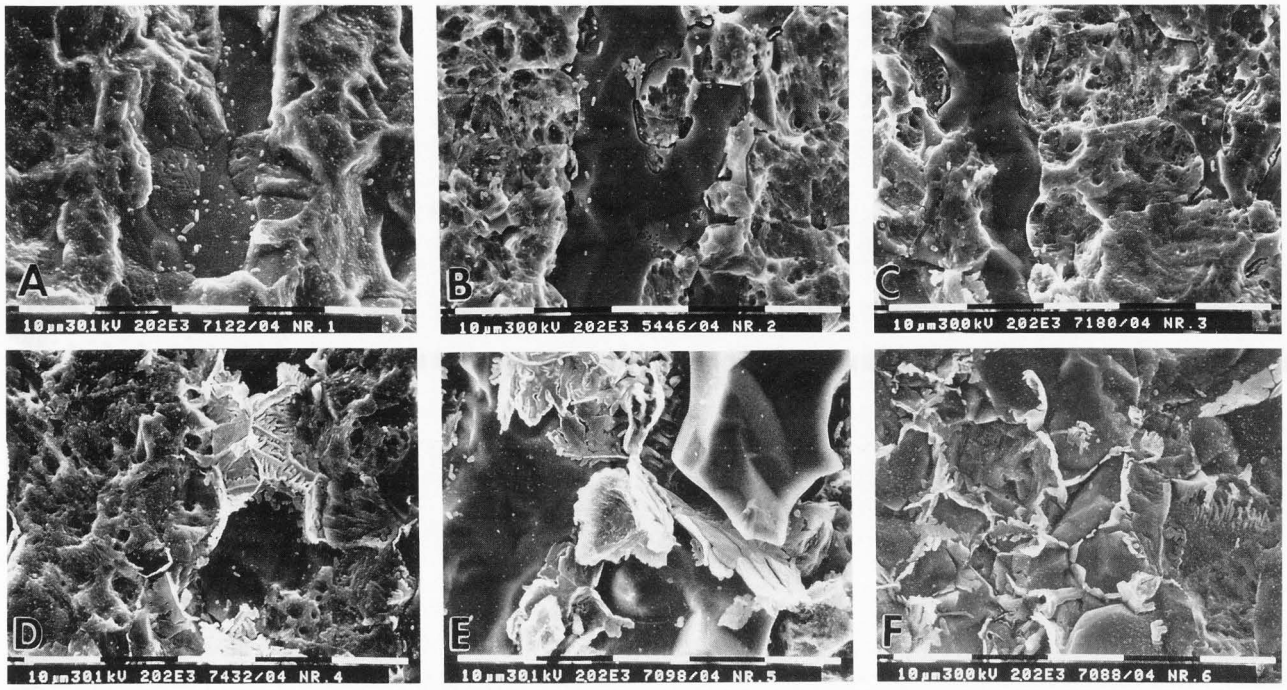

Fig.12. The SEM-micrographs of the deep etched samples according to Fig.11 (melt C5).

be explained by the formation of dendritic precipitations at the phase boundary between delta-ferrite and martensite.

After the fastest quenching, the delta-ferrite was covered by a few undissolved carbides, only. Phase boundary lining was not observed. With the beginning of the slower cooling rates, as indicated by the hatched area in the CCT diagrams of melt C4, C5 and C6, the phase boundaries were decorated with dendritic carbides. The same structure of carbides can be seen in the deeply etched CVN samples of the melts C4, C5 and C6. The dilatometer samples of melt C5 are shown in Figs.12 A-F. The letters of the SEM-micrographs correspond to those of the cooling curves in the CCT diagram of melt C5. Nothing will happen during the first cooling period from 1075°C to 600°C which takes about 10 min. During the following 10 min, the dendritic $M_{23}C_6$ located at the phase boundary grows until a temperature of 350°C is reached. This temperature marks the completion of the growing process.

Discussion

Two unexpected results were obtained by the impact tests:
1) The decrease of DBTT as a result of small delta-ferrite contents (0.5%),
2) A strong increase of cleavage brittleness at higher delta-ferrite contents.

On the basis of the microscopical investigations these results can be interpretate as follows:

The decisive factor for the initiation of a cleavage fracture could be the envelopment of the delta-ferrite phase by the dendritic carbide precipitates. Carbide envelopment increases with increasing delta-ferrite quantities. This can cause a crack in the delta-ferrite during dynamic loads, which is most likely initiated by the grain boundary carbides.

The favourable effect of smaller delta-ferrite contents (0.5%) can also be explained. Only a few carbides are formed on the phase boundary of the delta-ferrite. The two phases are not divided by a carbide wall. The soft delta-ferrite has positive influence to the ductility of the material.

The assumption that DBTT is to increase with higher chromium content can be alleviated by investigations made in Japan (5). These experiments showed no remarkable effect on impact energy and DBTT of alloys with chromium contents of 3 and 15 wt.%.

Very often the idea is presumed that the dendrites would form in the melt only. But Cahn (3), however, described the formation of liquid, gas and solid state. It was proved by our investigations, that the dendrites in our laboratory melts originated from the solid state. The development of the dendrites in dependence of the CCT-curves has been found. Most important factor is the cooling rate after the austenitization. At high cooling rates, there is no time for dendritic formation. Below $\lambda = 6.6$ no diffusion of carbon is observed. There is no doubt

that the excess carbon is released by the delta-ferrite and that first precipitations are formed on the phase boundary during the above mentioned cooling process. These carbides serve as nuclei for fast dendritic growth.Then, more carbon diffuses from the austenite, and the austenite around the carbides is transformed into ferrite. Between these two phases, a high concentration of carbides occurs. The boundary of the delta-ferrite will be covered by the dendritic $M_{23}C_6$ with the newly formed ferrite in between.

The phenomenon can be explained by discontinuous precipitation (4). In the CCT diagrams of the melts C4, C5 and C6 (>11 wt.% chromium) hatched areas are marked. They indicate the time of growth of the carbide/ferrite system. The most important mechanism must be carbon diffusion. The hardness values decrease which is one prerequisite for less dissolved carbon in the matrix. The measured values were confirmed by approximate diffusion calculation.

Acknowledgements

The author feels indebted to Dr.H.Finkler, Saarstahl GmbH, Völklingen, Federal Republic of Germany, for carrying out the dilatometer measurements and designing the CCT diagrams. Also, the author thanks Dr.K.Anderko and Prof.K.Ehrlich for the helpful discussions, and Mrs.Tiedau for assistance in preparing this work.

References

1. Abe F, Araki H, Okada M (1988) Microstructure and toughness of Cr-W and Cr-V Ferritic Steels. J.Nucl.Mat., Vol.155-157, 656-661.

2. Anderko K, David K, Ohly W, Schirra M, Wassilew C (1984) Optimization Work on Niobium Stabilized 12% CrMoVNb Martensitic Steels for Breeder and Fusion Reactor Application. Proc.Top.Conf. on Ferritic Alloys for Use in Nuclear Energy Technologies, Snowbird, U.T., USA. J.W.Davis, D.J.Michel, eds., The Metall.Soc.of AIME, 299-306.

3. Cahn R W (1974) Physical Metallurgy. North-Holland publishing Company, 434-437.

4. Hornbogen E (1979) Werkstoffe: Aufbau und Eigenschaften von Keramik, Metallen, Kunststoffen und Verbundwerkstoffen (Materials: Structures and Properties of Ceramics, Metals Synthetics and Composites), 2. neubearb. u. erw. Aufl. Springer New York, 90-93.

5. Kayano H, Kimura A, Narui M, Sasaki Y, Suzuki Y, Ohta S (1988) Irradiation Embrittlement of Neutron-Irradiated Low Activation Ferritic Steels. J.Nucl.Mat. Vol.155-157, 978-981.

6. Klueh R L, Maziasz P J (1988) Reduced-Activation Ferritic Steels: A Comparison with Cr-Mo-Steels. J.Nucl.Mat. Vol.155-157, 602-607.

7. Krainer E, Scheidl H (1977) Einfluss des Deltaferritgehaltes auf die mechanischen Eigenschaften der 12%igen Chromstähle sowie Dämpfungsuntersuchungen an Turbinenschaufelwerkstoffen (The Enfluence of the Delta-Ferrite Content on the Mechanical Properties of the 12% Cr-Steels and the Investigations of Mechanical Resistance of Turbine Blade Material), Radex-Rundschau, Heft 3, Österreichisch-Amerikanische Magnesit A.G., 246-268.

8. Little E A, Harries D R, Pickering F B (1978) Some Aspects of the Structure-Property Relationships in 12% Cr Steels. In: Ferritic Steels for Fast Reactor Steam Generators, Proc.Intern.Conf., British Nuclear Energy Society, London, 136-144.

9. Little E A, Harries D R, Pickering F B, Keown S R (1977) Effects of Heat Treatment on Structure and Properties of 12% Cr Steels, Metals Technology 4, 205-217.

10. Loria E A (1961) Influence of Delta-Ferrite Carbide Segregates on the Properties of 12% Chromium Steel. Trans.ASM 54, 31-49, 705-719.

11. Materna-Morris E, Schirra M, Ehrlich K (1987) The Correlation Between Fracture Behaviour and Microstructure in a Nb-Bearing, Fully Martensitic Steel of Type 1.4914. In: Materials for Nuclear Reactor Core Applications, Proc.Intern.Conf., Vol.1, British Nuclear Energy Society, London, 263-269.

12. Materna-Morris E, Schäfer L, Anderko K (1989) Der Einfluss der Delta-Ferritphase auf das Bruchverhalten von 9-14% Chromstählen im instrumentierten Kerbschlagversuch (The Enfluence of the Delta-Ferrite Phase on the Fracture Behaviour of 9-14% Chromium-Steels during Instrumented Impact Tests). Berichte der Metallographie-Tagung Garmisch-Partenkirchen 28.-30.September 1988. In: Petzow G, Sonderbände der Metallographie, Bd.20, Dr.Riederer-Verlag GmbH, Stuttgart, 283 - 294.

13. Schirra M, Schäfer L, Anderko K (1988) Instrumentierte Kerbschlagbiegeversuche sowie Zug- und Zeitstandversuche an einem martensitischen Chromstahl mit unterschiedlichen Deltaferritgehalten (Instrumented Impact Tests and Tensile- and Creep-Tests of a Martensitic Chromium-Steel with Different Delta-Ferrite Contents), Vorträge der Tagung: Werkstoffprüfung 1988, Bad Nauheim. Deutscher Verband für Materialprüfung, 375-383.

Discussion with Reviewers

V.Thien: Figure 5: Where is "cleavage fracture" visible in the polished cross-section? Where and how can one see that dimples occur at grain boundary carbides? You mention a transcrystalline mixed fracture type; does it not require large part of dimple areas?
A.Vasilev: Are there dimpes between cleavage areas indeed (in Fig.5A)?
Author: The cleavage fracture can be seen in Fig.5A at the areas marked 'δ--ferrite'. In the polished microsection (Fig.5B) the cracks in the delta-ferrite are visible. These cracks cause plain fracture surfaces.

You are right, a transcrystalline mixed fracture type requires a large part of dimple areas. I chose a picture with a higher magnification and with more cleavage areas. There, I analysed the delta-ferrite parts of the fracture surface.

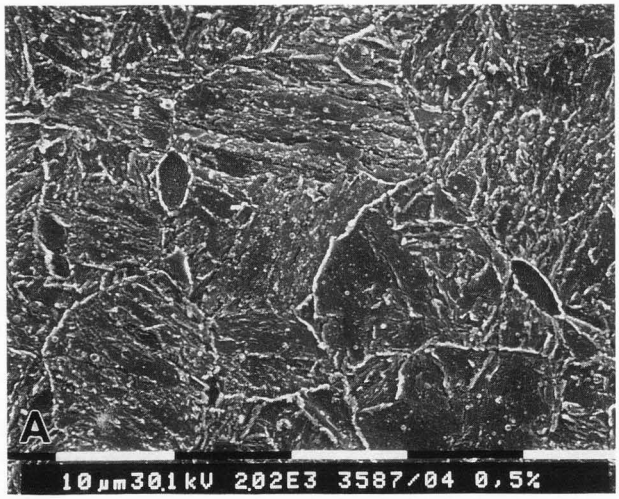

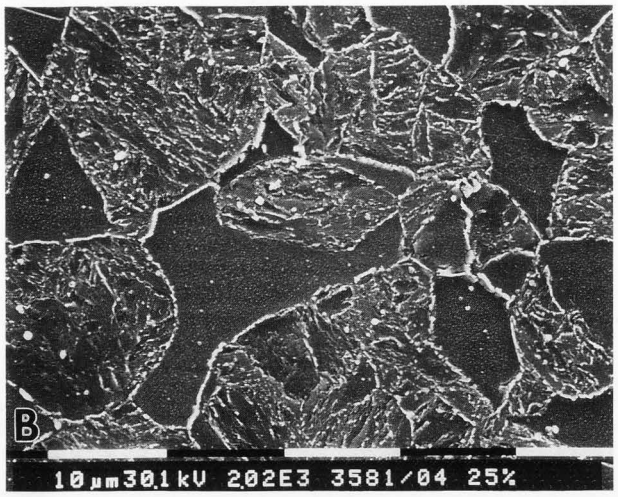

Fig.13. Two SEM micrographs of metallographic cuts.

The dimple parts can be found mostly in the drops of the crack propagation lines, e.g., as can be seen in the small picture of Fig.3. The dimples around the particles can be seen only in the ductile parts of the fracture as shown in Fig.4B.

V.Thien: The prior austenitic grain sizes in all melts should be in the order of 30±10 µm diameter; can you prove it?
Author: The micrographs in this paper show deformed materials from which it is difficult to get an idea of the real grain size of the prior austenit. We prepared metallographic cuts and investigated them by light microscopy and SEM. Two SEM-micrographs (Fig.13) of melts C3 and C6 show the prior austenitic grains.

V.Thien: Hardness increases more with chromium content and other carbides, up to 12 wt.% Cr (5% delta-ferrite). With higher delta-ferrite parts, hardness decreases because of higher parts of soft ferrite phase.
Author: With the results of the hardness, we thought the soft delta-ferrite would influence positively the DBTT-values, as we found in the melt with 5% delta-ferrite. But we could prove the influence of the soft phase is lost in the melts with higher chromium content and the formation of the massive carbides around the delta-ferrite.

Reviewer I: Is the author sure that the morphology of the delta-ferrite is the same for all casts and that the only parameter varying is the volume fraction of delta ferrite?
Author: We analysed the chemical compositions by EDX in STEM, too. We detected Fe and Cr. In the melt C3 the chromium content of delta-ferrite was about 1 wt% higher than in martensite. This chromium content difference increases up to 2.5 wt% in melt C6. The carbon content could not be analysed by microprobe because the carbides influenced the measurements.

Reviewer I: Does the fixed tempering treatment of 2h/ 700°C produce identical changes in dislocation structure in the martensite with varying Cr contents?
Author: We did not analyse the changes in dislocation structure. This would be a good evidence about the internal stresses. We measured only the hardness, as shown in Fig.7.

Reviewer I: What was the purpose of using instrumented impact tests since only the total absorbed energy values were used?
Author: This paper describes more the microstructural and fractographical changes than the mechanical tests.We have written a separate paper about the mechanical behaviour and the instrumented impact

tests: Anderko A, Schäfer L, Materna-Morris E; Effect of the delta-ferrite phase on the impact properties (will be published in Proc: 4th Internat.Conf.on Fusion Reactor Materials, December 4-8, 1989, Kyoto, Japan).

A.Vasilev: What points to a connection of dimples with boundary carbides? What mechanism of pore initiation takes place in this case? Isn`t it the intergranular dimple fracture?
Author: The dimples are formed around the big carbides of delta-ferrite/martensite boundary, Fig.4B. They loose their connection with the matrix during the deformation. This effect can be intensified by the different elasticity behaviours of the two phases. In this case, we have an intergranular dimple fracture, but this is only for the delta-ferrite and not for the martensite.

During the transission to more brittle fracture portions, we observed the cracks in the dendritic carbides and in the delta-ferrite. Then, the fracture of the delta-ferrite changed to cleavage fracture.

We assume, the energy during crack propagation is stored in the carbides and the energy can be released promptly to the delta-ferrite.The formation of cleavage fracture depends also on the fracture velocity.